Catena 76 (2009) 173–181

Contents lists available at ScienceDirect

Catena

journal homepage: www.elsevier.com/locate/catena

Field measurement of infiltration rate using an oscillating nozzle rainfall simulator in the cold, semiarid grassland of Mongolia

H. Kato [a,*], Y. Onda [a,1], Y. Tanaka [b], M. Asano [a]

[a] Graduate School of Life and Environmental Sciences, University of Tsukuba, 1-1-1 Tennodai, Tsukuba, Ibaraki 305-8572, Japan
[b] Department of Geography, Kyung Hee University, Seoul 130-701, Republic of Korea

ARTICLE INFO

Article history:
Received 28 May 2008
Received in revised form 11 November 2008
Accepted 18 November 2008

Keywords:
Semiarid grassland
Mongolia
Infiltration rate
Rainfall simulation
Surface cover

ABSTRACT

Recent intensive grazing in Mongolia may be significantly reducing the infiltration rate of rangeland. This study measured infiltration rates using simulated rainfall with high raindrop impact for small plots established on steppe grassland, desert grassland, and shrubland sites in Mongolia. The response of the infiltration rate to short-term livestock removal was also investigated. On the steppe grassland, a high infiltration rate was measured on an ungrazed plot with relatively dense vegetation cover; a statistically significant correlation was found between the total surface cover and final infiltration rate, indicating that surface cover by rock fragments also increased the infiltration rate to some extent. For desert grassland and shrubland, however, the surface cover condition was not a major factor controlling the final infiltration rate. After 4 years of livestock removal, the surface vegetation cover of the ungrazed plot was greater than that of the grazed plot, but no appreciable change occurred in soil penetration resistance. These results suggest that the high infiltration rate on the ungrazed plot was maintained mainly by the recovery of surface vegetation cover after the short-term livestock removal; this may indicate a potential mechanism of recovery from desertification processes for Mongolian rangeland.

1. Introduction

Mongolia is located in northeastern Asia, and approximately 75% of its total land area consists of cold, semiarid grassland that is subjected to grazing throughout the year (Begzsuren et al., 2004). Grazing, the cold climate, and the short growing period have led to sparse plant cover in the grasslands of Mongolia (Munkhtsetseg et al., 2007). Currently, Mongolian grasslands, particularly the desert grasslands of southern Mongolia (Bayasgolan and Dagvadorj, 2005), are considered to be in the process of desertification caused by overgrazing (Chuluun and Ojima, 2001). The rise in livestock numbers since Mongolia's development of a market-oriented economy may affect the growth, density, and distribution of grassland plants (Chen et al., 2006), which may in turn lead to a drastic increase in soil erosion (Onda et al., 2007). However, the process of desertification due to overgrazing in this region is not yet fully understood.

In arid and semiarid rangelands, the process of desertification due to overgrazing has been described in terms of changes in surface vegetation and reduction in the infiltration rate (Rietkerk et al., 2000). In general, the soil in a semiarid area has a low organic content and large percentage of silt portions, which results in high soil susceptibility to surface sealing and crusting (Abu-Awwad and Shatanawi, 1997; Mills and Fey, 2004). Thus, the loss of surface vegetation cover decreases the infiltration rate significantly because the direct kinetic energy impact of raindrops on a bare surface promotes the development of surface sealing and crusting (Evans, 1980). Thus, the recent overgrazing in Mongolia may be reducing the infiltration rate of the grassland.

On semiarid grasslands, the relationship between the surface vegetation cover and infiltration rate has been examined by means of field rainfall simulation experiments on the prairies of North America (Blackburn, 1975; Dadkhah and Gifford, 1980; Thurow et al., 1986; Gutierrez and Hernandez, 1996), Mediterranean ecosystems (Cerdà et al., 1998; Seeger, 2007), and rehabilitated grassy hillslopes in Australia (Loch, 2000a). The results of these rainfall simulation experiments have demonstrated positive relationships between surface vegetation cover and infiltration rate. However, on the grassland of Mongolia, although some runoff data were collected on a hillslope plot (Onda et al., 2007), very few data on the infiltration rate are currently available. Therefore, the role of surface vegetation cover in the infiltration rate in this region is not yet sufficiently understood.

Reduction of the infiltration rate increases overland flow generation and surface erosion, which results in the increase of sediment and nutrient loss (Schlesinger et al., 1999; Brazier et al., 2007) and a

* Corresponding author. Tel./fax: +81 29 853 7189.
E-mail addresses: hiroakis980@ybb.ne.jp (H. Kato), onda@geoenv.tsukuba.ac.jp (Y. Onda), ytanaka@khu.ac.kr (Y. Tanaka), asano@a5.keio.jp (M. Asano).
[1] Tel./fax: +81 29 853 7189.

0341-8162/$ – see front matter © 2008 Elsevier B.V. All rights reserved.
doi:10.1016/j.catena.2008.11.003

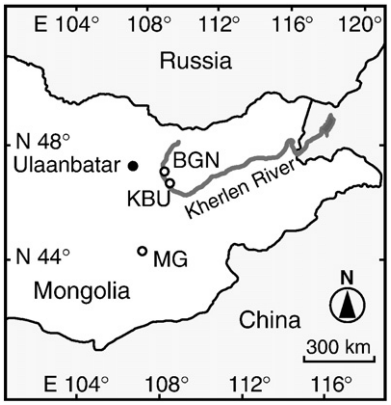

Fig. 1. Map of the study area.

decrease in plant available soil water (Rietkerk et al., 2000). Such changes have been considered primary causes of the change in dominant vegetation type from grassland to shrubland (Wainwright et al., 2000; Ritchie et al., 2003) as part of the so-called desertification process. On the semiarid grassland of the Jornada Long Term Experimental Range (LTER), southern New Mexico, where such a transition of surface vegetation has occurred over the last hundred years, the process is considered to be largely irreversible (Hennessy et al., 1983; Gibbens et al., 1992). It has been thought that the infiltration rate does not recover unless surface vegetation cover recovers; however, in San Simon Valley in southern Arizona, the infiltration rate of degraded grassland increased, primarily due to recovery from livestock-induced soil compaction after long-term livestock removal (Castellano and Valone, 2007). However, in this case, the infiltration rate was measured using a double-ring infiltrometer, which does not simulate the raindrop impacts of rainfall; thus the infiltration rate may not have sufficiently recovered because the surface vegetation cover had not recovered at that site. Investigating the response of the infiltration rate to livestock removal is essential to understanding potential mechanisms of recovery from desertification on degraded rangelands; however, such investigation has been hampered by the lack of infiltration-rate field data.

To address this problem, we carried out a series of field infiltration tests for various surface cover conditions using a modified rainfall simulator and small plots (1 m^2). In addition, we conducted a comparative analysis of infiltration rates between a site with short-term livestock exclusion and a site with year-round open range grazing. The objectives of this study were to elucidate the fundamental relationships between surface vegetation cover and infiltration rate on steppe, desert grassland, and shrubland and to determine the effect of short-term livestock exclusion on the recovery of the infiltration rate for steppe grassland.

2. Study sites

The sites selected for this study were located in steppe and desert steppe regions of Mongolia (Fig. 1). One study area was in Khentii Province, 100 km east of Ulaanbaatar, and featured steppe grassland with tall-grass prairie. The other was in Mandalgobi in Dundgobi Province, 250 km south of Ulaanbaatar, and was covered by desert grassland with short grasses and shrubs. Both study areas have been subjected to grazing by domestic livestock under nomadic and seminomadic patterns of land use. Sheep, goats, cattle, and horses are typical livestock in these areas.

In Khentii Province, the experimental sites were selected in two regions having different grazing conditions (according to data provided by the Statistical Office of Mongolia): Kherlen-bayan Ulaan (KBU; 47°13′N, 108°44′E) and Baganuur (BGN; 47°40′N, 108°29′E). These areas have a cold, semiarid climate with an annual mean temperature of 2 °C (data provided by the Institute of Meteorology and Hydrology, Ministry of Nature and Environment, Mongolia). Average annual precipitation over the 11 years from 1993 to 2003 was 181 mm for the KBU region and 213 mm for the BGN region (Sugita et al., 2007). Most (>80%) of the annual precipitation occurs during the warm rainy season between June and September, and the hilly land is used for pastures. Sandstone and granite underlie the KBU and BGN sites,

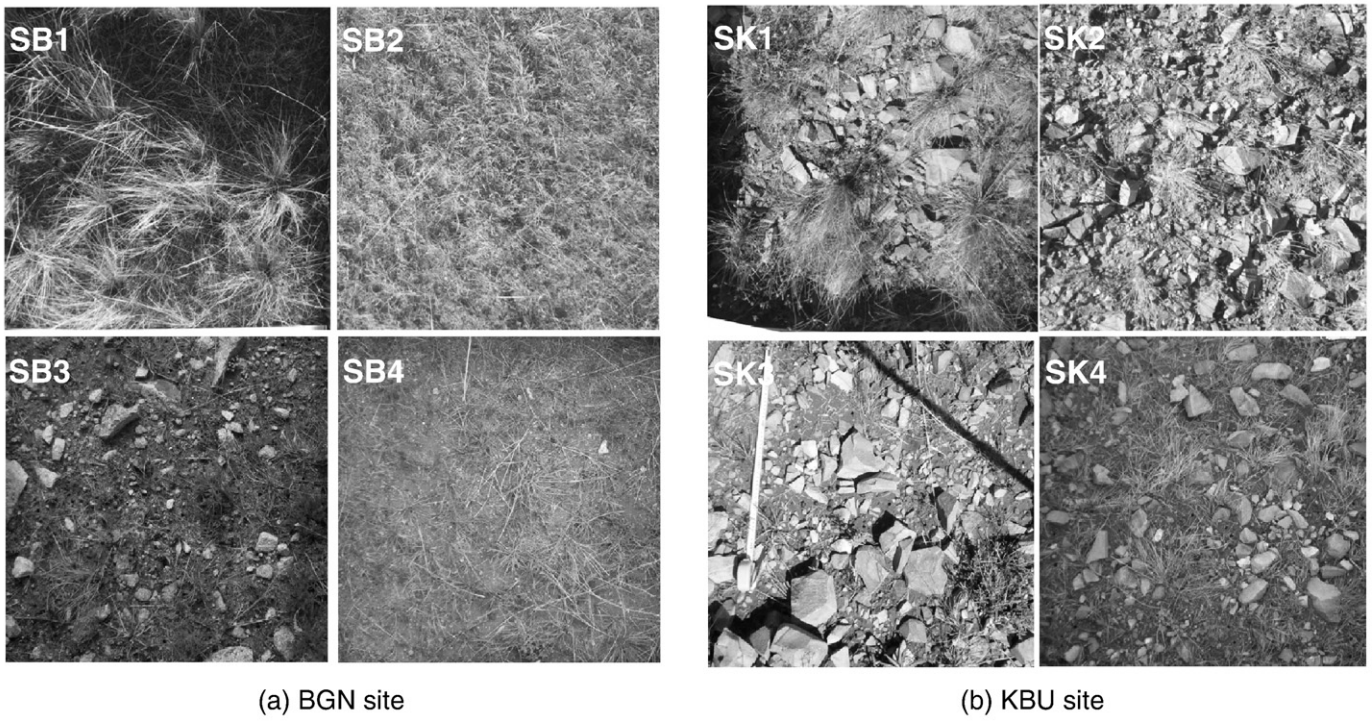

Fig. 2. Surface conditions of the experimental plots in the steppe grassland.

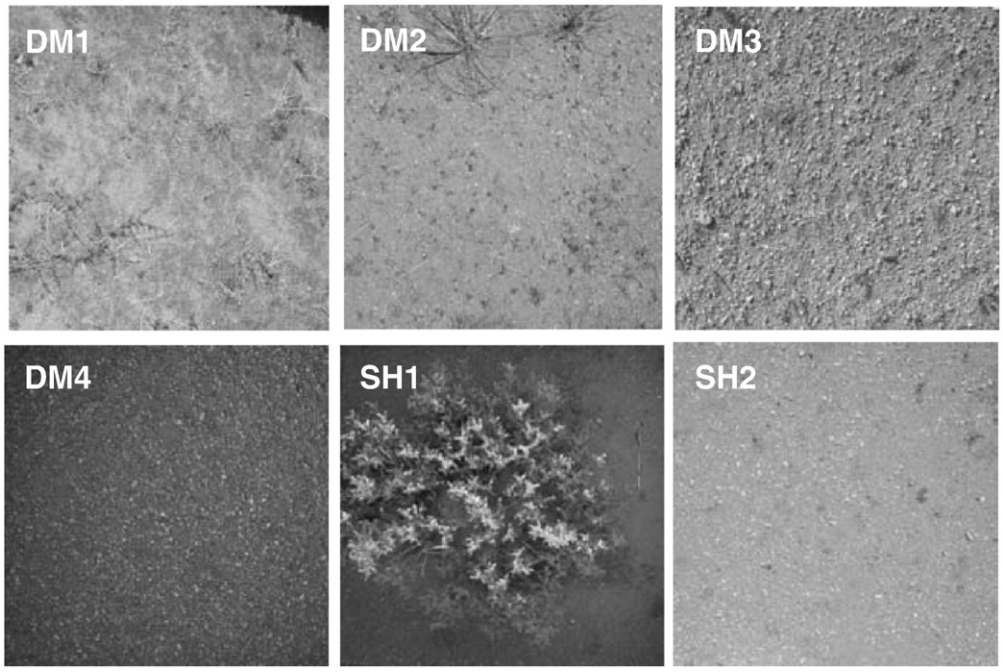

Fig. 3. Surface conditions of the experimental plots at the desert grassland and shrubland sites.

respectively. Soil at both sites is Calcic Kastanozems (Asano et al., 2007), and the steppe grassland is dominated by perennial grasses and forbs. The dominant grass species were *Stipa krylovii* and *Carex* sp. at KBU and *Leymus chinensis*, *S. krylovii*, and *Kochia prostrata* at BGN (Asano et al., 2007). The grassland at KBU has long served as a winter shelter for livestock and has thus been subjected to intensive grazing. At BGN, livestock numbers have increased considerably since the development of the market economy in 1990–1991. Given these conditions, we could expect declines in grassland at these study sites.

On the steppe grassland, eight sites were selected for the rainfall simulation experiment. Fig. 2 shows the surface cover conditions of each plot. Ungrazed sites (SB1, SK1) and grazed (SB2, SK2) sites were prepared at BGN and KBU. The ungrazed and grazed sites were situated alongside each other on slopes of 15° gradient. The grazed sites had been subjected to year-round patterns of grazing. For the ungrazed sites, livestock had been excluded for the previous 4 years by enclosing the sites with 1.5-m-high fences. Additional plots were also established on backslope (SB3, SK3) and footslope (SB4, SK4) locations to obtain plots with different grades of surface vegetation cover. The KBU and BGN sites had backslope gradients of 22° and 19° and footslope gradients of 15° and 13°, respectively. For both the BGN and KBU sites, analysis of the ^{137}Cs inventory in the surface soil suggested that intensive soil erosion occurred on the backslopes, whereas little soil erosion or sediment deposition occurred on the footslopes (Nishikawa et al., 2005).

The Mandalgobi region has an annual mean temperature of approximately 3 °C, and the annual mean precipitation over the 11 years from 1993 to 2003 was 162 mm (data provided by the Institute of Meteorology and Hydrology, Ministry of Nature and Environment, Mongolia). The annual precipitation varies considerably from year to year. The majority (>80%) of the annual precipitation falls during the rainy season in summer. The area generally has flat land and gently sloping hills as landforms, and light chestnut soil (Saandar and Sugita, 2004). The dominant grass species are *Stipa glareosa* and *Artemisia frigida* (Munkhtsetseg et al., 2007). Surface vegetation cover is very scattered, and even in the ungrazed location where livestock have been excluded for a long period, cover is less than 20%. No field data on the infiltration rate are currently available for this area; however, traces of water flow along hollows provide evidence of overland flow generation during a storm rainfall event.

For the desert grassland and shrubland in Mandalgobi, we selected six sites for the rainfall simulation experiment. The slope gradient of each plot ranged from 3° to 5°. Fig. 3 shows the surface cover conditions of the plots. Since Mandalgobi airport (1950 m×140 m) was surrounded by a fence to keep out livestock, we selected an area inside the airport grounds as an ungrazed location. The airport grounds had very scattered patches of grasses and forbs. We established one plot on the west side of the airport (DM1), where accumulations of sandy aeolian deposits formed sandy micromounds on the surface. We established another plot on the east side of the airport (DM2), which had fewer micromounds compared to the west side. In grazed areas outside the airport fence, we established one plot (DM3) adjacent to the airport and another plot (DM4) 15 km south of Mandalgobi City. The shrubland site was located approximately 15 km northwest of Mandalgobi City. *Caragana microphylla* was the dominant shrub. Sandy soil accumulated beneath the shrubs, while the surface of the intershrub area was flat and almost bare. The rainfall simulation experiment was conducted on both shrub (SH1) and intershrub (SH2) plots.

3. Materials and methods

3.1. Rainfall simulation experiment

On semiarid grassland of Mongolia, Onda et al. (2007) found that overland flow usually occurred only with a high raindrop impact exceeding approximately 40 J m^{-2} min^{-1}. In a laboratory experiment, the final infiltration rate decreased as the raindrop kinetic energy increased (Agassi et al., 1994). Therefore, to evaluate the infiltration rate of semiarid grasslands of Mongolia, generating high raindrop impacts like those found during rainstorms is necessary. In this study, we developed a modified, lightweight rainfall simulator based on the design used by Meyer and Harmon (1979). A flat fan Veejet 80150 spraying nozzle (Spraying Systems Co., Wheaton, IL), which was mounted on the manifold at a height of 2.13 m from the plot surface, oscillated so that the spray fans swept across the target plot (Fig. 4). The Veejet 80150 spraying nozzle can produce raindrops larger than 2 mm in diameter (Meyer and Harmon, 1979). Raindrops that were not applied within the target plot were recycled via the droplet catch trays

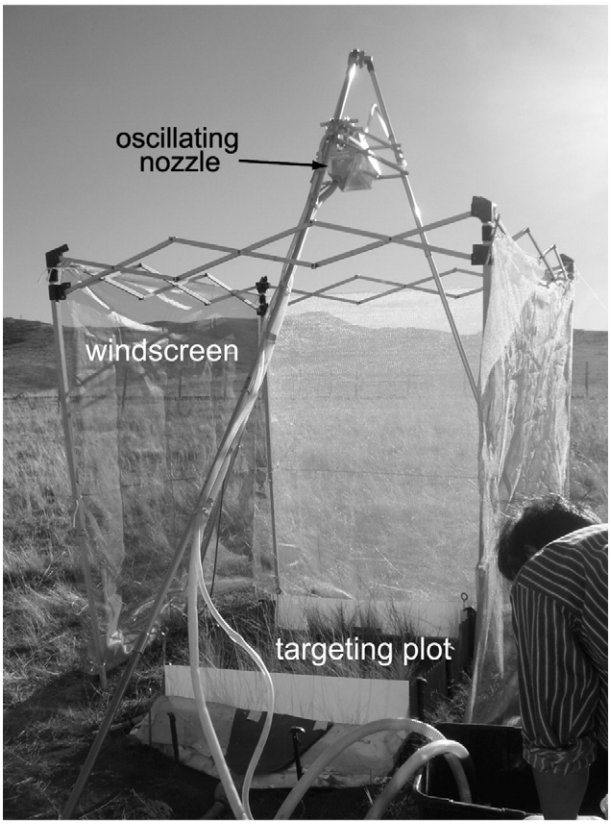

Fig. 4. Modified oscillating nozzle rainfall simulator.

on either side of the spraying nozzle. One-half of the sprinkled rainfall fell onto the target plot, and the remaining half fell on a buffer zone approximately 30 cm outside the boundary walls of the target plot. Establishment of a buffer zone and a windscreen can minimize the influence of wind on the constant intensity of simulated rain. The flow rate of water to the spraying nozzle was controlled in the range of 12.0–12.5 L min^{-1} using a water valve and a digital flow meter (LF10-PTN; HORIBA STEC Co., Ltd., Kyoto, Japan).

The performance of the modified rainfall simulator used in this study was well tested (Kato et al., in press). The coefficient of variability (CV) and the distribution uniformity (DU) of rainfall intensity for the modified rainfall simulator were 86.9% and 80.7%, respectively. The median diameter of a simulated raindrop was 3.5 mm, and the raindrop kinetic energy of the simulated rainfall was 22.6 J mm^{-1}; these measurements were taken using a laser raindrop-sizing instrument (Nanko et al., 2004). When the rainfall intensity of simulated rainfall was 180 mm h^{-1}, the total raindrop kinetic energy of the simulated rainfall per unit area was 67.8 J m^{-2} min^{-1}. This is greater than the observed critical kinetic energy of natural rainfall (40 J m^{-2} min^{-1}), above which overland flow occurred on the Mongolian steppe grassland (Onda et al., 2007).

Ground surfaces are composed of various parts having different infiltration rates; therefore, surface runoff could occur under lower rainfall intensities on surfaces in which infiltration is less than average (Murai and Iwasaki, 1975). For this reason, generating excess rainfall over the entire surface is necessary to evaluate the mean infiltration rate of the ground surface (Dunne et al., 1991). Thus, we simulated high-intensity (170 mm h^{-1} and 200 mm h^{-1}) rainfall in this study. To measure the infiltration rate, a single rainstorm event was simulated at an experimental plot for 20–30 min; this simulation was reasonable because thunderstorms usually occur on dry soil in the study area. To minimize the influences of antecedent soil moisture, which may affect the observed final infiltration rate, comparative sets of rainfall simulation experiments were conducted on the same day or at least the next day of the first experiment. The surface runoff from the plot was hand-measured using a volumetric cylinder at 1-min intervals; following this, the infiltration rate was calculated by subtracting the surface runoff rate from the rainfall intensity of the simulated rain.

3.2. Experimental plots for the rainfall simulation experiments

Each small plot used for the rainfall simulation experiments had an area of 1 m^2 (1 m × 1 m). Its upslope and lateral boundaries were edged by 25-cm-high corrugated walls, which were pushed 5 cm into the soil to minimize surface soil disturbance. The gaps between the wall and the soil were filled with fine soil particles to avoid water leakage. The wavy shape of the boundary wall prohibited the surface flow from running down along the lateral boundary wall. At the downside boundary of the plot, a metal flume was inserted laterally 5 cm into the soil to avoid the leakage of inflow and to permit measurement of the surface flow rate from the plot.

3.3. Measurement of surface cover

Experimental plots with a wide range of surface vegetation covers were established for the rainfall simulation experiment. The cover percentages of vegetation, rock fragments, and bare surface within each plot were estimated visually from photographs. A rock fragment of approximately 3.6 mm (5 pixels on the image) or larger in diameter was defined as stone cover. The penetration resistance of the surface soil (<5 cm) was measured using a push-cone penetrometer (DIK-5561; Daiki Rika Co., Ltd., Tokyo, Japan). Measurements of penetration resistance were taken on the surface (1 m^2) adjacent to each plot to avoid surface disturbance of the plot for the rainfall simulation experiment. The particle size distributions of topsoil were analyzed using the sieve method (>450 μm) and a laser diffraction particle size analyzer (SALD-3100; Shimadzu Co., Ltd., Kyoto, Japan).

4. Results

4.1. Plot surface characteristics

Table 1 lists the study sites, their cover percentages of vegetation, rock fragments, and bare surface, and their slope gradients. For the steppe grassland, the surface vegetation cover of the experimental plots ranged from 16.6 to 91.7% for the BGN site and from 10.1 to 46.7%

Table 1
Surface cover characteristics and slope gradient of the experimental plots for rainfall simulation experiments on the steppe grassland, desert grassland, and shrubland sites

Site name	Vegetation (%)	Stone (%)	Bare (%)	Slope (degrees)
Steppe grassland				
Baganuur (BGN)				
SB1	91.7	0.0	8.3	15
SB2	28.0	0.0	72.0	15
SB3	16.6	11.3	72.1	22
SB4	39.3	0.4	60.3	15
Kherlen-bayan Ulaan (KBU)				
SK1	46.7	20.5	32.8	15
SK2	22.1	31.3	46.6	15
SK3	10.1	42.7	47.2	19
SK4	18.7	19.6	61.7	13
Desert grassland/shrubland				
Mandal Gobi (MG)				
DM1	16.6	0.4	83.0	5
DM2	9.0	16.3	74.7	4
DM3	1.6	16.3	82.1	5
DM4	0.7	25.9	73.4	3
SH1	34.8	9.4	55.8	4
SH2	0.1	13.3	86.6	4

Table 2
Topsoil textures of the experimental plots at the steppe grassland, desert grassland, and shrubland sites

Site name	Clay (%)	Silt (%)	Sand (%)	Fine (%)	Oc (%)
Steppe grassland					
Baganuur (BGN)					
SB1	9.6	51.3	39.1	nd	8.3
SB2	9.6	56.8	33.6	82.6	8.0
SB3	6.7	25.1	68.2	64.7	5.5
SB4	9.6	27.2	63.2	94.1	7.4
Kherlen-bayan Ulaan (KBU)					
SK1	12.2	47.4	40.3	nd	8.5
SK2	13.3	43.4	43.3	76.9	8.3
SK3	15.8	30.0	54.2	46.7	6.5
SK4	15.9	29.6	54.5	67.7	7.7
Desert grassland/shrubland					
Mandalgobi					
DM1	8.0	14.7	77.3	92.5	2.2
DM2	13.4	36.7	50.0	83.7	3.0
DM3	16.4	34.6	49.0	72.9	2.5
DM4	19.5	46.7	33.8	79.3	3.3
SH1	0.0	0.0	100.0	99.6	1.8
SH2	2.9	5.4	91.7	91.2	7.6

"Fine" indicates the fraction of particles smaller than 2 mm in diameter, and "Oc" represents the organic matter content.

for the KBU site. The highest vegetation cover was found on the ungrazed plots (SB1, SK1), and the surface vegetation cover for the footslope plots was higher than that of the backslope plots at both sites. The topsoil at KBU was characterized by a stony surface, while the rock fragment cover at BGN was limited to summit positions and steep backslopes. The surface vegetation for the KBU site was relatively sparse; however, the area of bare surface was less than that of the BGN site because of the surface rock fragment cover. The topsoil at all the steppe grassland sites was silty–sandy soil (Table 2). Although topsoils at KBU had slightly higher clay and gravel content than those at BGN, overall, the soil textures were similar to each other.

For the desert grassland, the surface vegetation covers for the ungrazed plots (DM1 and DM2) were 16.6 and 9.0%, respectively, whereas the ground surface of the grazed plots was almost bare, with surface vegetation cover below 2% (Table 1). The topsoil was mostly silty–sandy soil although the sand content for the plot with micro-mounds (DM1) was very high (Table 2). In the shrub plot, shrub canopies were approximately 60 cm in diameter and covered 34.8% of the total surface area of the plot, with interdune areas covering the remainder. The topsoil of the shrub and intershrub plots mostly consisted of sand particles.

4.2. Temporal variation in the infiltration rate

Fig. 5 shows temporal changes in infiltration rates measured on the steppe grassland. At both BGN and KBU, the infiltration curves show different patterns for the ungrazed and grazed plots (Fig. 5a). For the BGN site, the infiltration rate at the ungrazed plot (SB1) decreased rapidly in the first 5 min; thereafter, it leveled off and showed marked fluctuations until the end of the experiment. At the grazed plot (SB2), the initial decline in the infiltration rate was slower than that at SB1 and showed a continuous decrease throughout the experiment. For the KBU site, the infiltration rate at the ungrazed plot (SK1) neared equilibrium in the first 10 min after the onset of simulated rainfall. At the grazed plot (SK2), the infiltration rate rapidly decreased in the first 5 min and thereafter decreased continuously at a constant rate until the end of the experiment. On the grazed plots, SB2 and SK2, infiltration rates failed to achieve equilibrium during the rainfall simulation experiments.

The infiltration curves for the backslope and footslope plots at BGN and KBU are shown in Fig. 5b. For the BGN site, the infiltration rate declined more rapidly at the footslope plot (SB4), but SB4 and SB3 had similar curve shapes until 15 min. Thereafter, the infiltration rate for SB4 reached equilibrium, whereas at SB3, the initial decline in the infiltration rate was followed by an increase. For the KBU site, the plots with different hillslope locations showed very similar infiltration curves; initial declines in the infiltration rate in the first 15 min were followed by increased rates toward the end of the experiment.

On desert grassland, the infiltration curve patterns varied considerably among the plots (Fig. 6a). All infiltration curves for desert grassland showed initial rapid declines. Thereafter, the infiltration rates for the DM1 and DM4 plots fluctuated and decreased toward the end of the experiment. For the DM2 and DM3 plots, initial declines in the infiltration rates were followed by rate increases. On the shrubland, the patterns of the infiltration curves were similar between the shrub plot (SH1) and the intershrub plot (SH2), although an earlier decline in the infiltration rate was observed for the shrub plot (Fig. 6b).

5. Discussion

5.1. Final infiltration rates for each experimental plot

The infiltration rates in the last 3 min of the simulated rainfall experiment were averaged for each plot. The results were as follows: 91.6 and 34.9 mm h^{-1} for the ungrazed and grazed plots at BGN; 100.3 and 39.9 mm h^{-1} for the ungrazed and grazed plots at KBU; 94.0 and

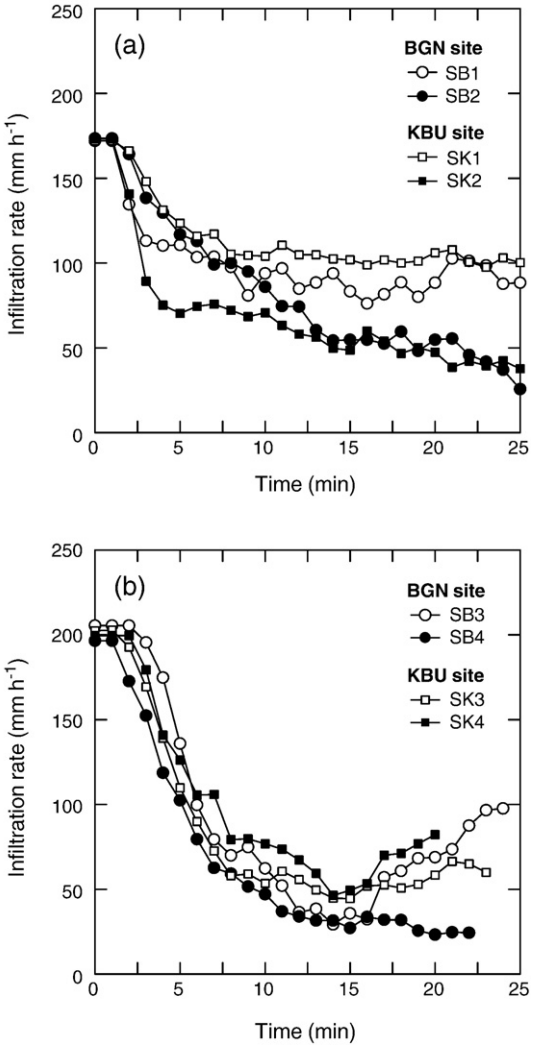

Fig. 5. Infiltration curves for the steppe grassland: (a) ungrazed and grazed sites; (b) backslope and footslope sites.

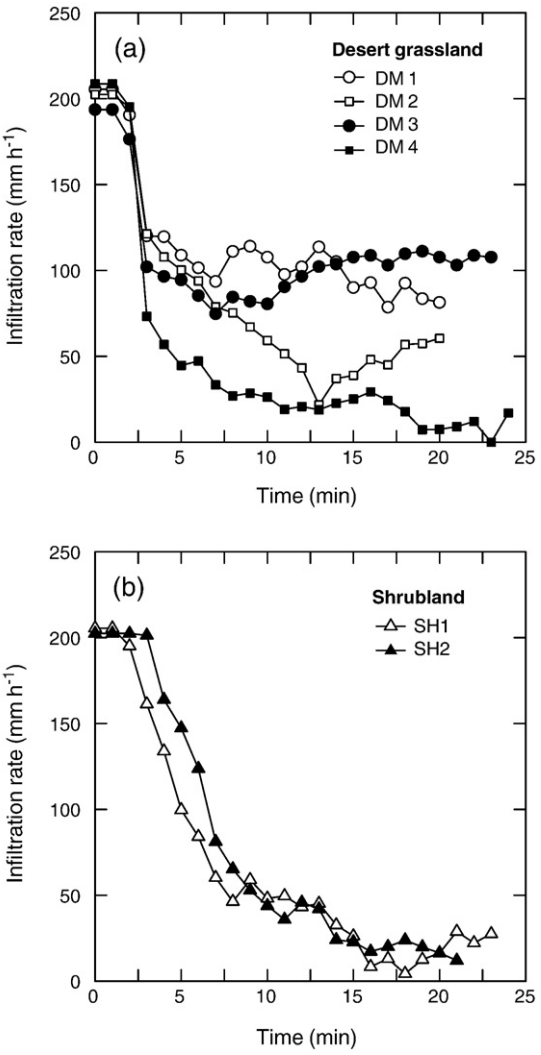

Fig. 6. Infiltration curves for the (a) desert grassland and (b) shrubland sites.

24.1 mm h^{-1} for the backslope and footslope plots at BGN; and 63.8 and 76.7 mm h^{-1} for the backslope and footslope plots at KBU, respectively. Desert grassland and shrubland had resulting values of 85.9 mm h^{-1} at DM1 and 58.3 mm h^{-1} at DM2; for the grazed locations, values were 106.5 mm h^{-1} at DM3 and 9.7 mm h^{-1} at DM4. The shrub plot and intershrub plot had values of 26.2 and 16.2 mm h^{-1}, respectively.

For the ungrazed plot SB1 at the BGN site, the infiltration rate showed marked fluctuations during the rainfall simulation experiment. Abrahams et al. (1988) observed marked fluctuations in surface runoff on degraded grassland hillslopes during a rainfall simulation experiment; they attributed this fluctuation to temporary formations of litter dams. In this study, the dry weight of litter material within a plot was 227 g m^{-2} for the ungrazed plot (SB1) and 50 g m^{-2} for the grazed plot (SB2). Thus, temporary dams formed by dead herbaceous materials may have occurred at plot SB1, leading to the observed fluctuations in the infiltration rate. Consequently, the 3-min average of the minimum infiltration rate (80.4 mm h^{-1}) during the simulated rainfall experiment was used as the final infiltration rate for SB1, instead of the mean infiltration rate for the last 3 min of the experiment.

The infiltration rates for some plots reached an early minimum and then increased in the latter half of the experiment. One possible explanation for the subsequent infiltration-rate increase was that loose litter and/or eroded soil particles trapped by obstacles in the overland flow path might have formed debris dams, which would have increased the infiltration rate by damming overland flow and increasing the surface storage capacity. Several studies have reported the influence of litter dams on surface runoff (e.g. Wainwright et al., 2000; Neave and Abrahams, 2002). These processes may have occurred during the rainfall simulation experiments in our study; however, it is doubtful that the volume of water trapped by debris dams would have been sufficient to account for the observed increase in the infiltration rate.

Another plausible explanation for the later increase in infiltration rates involves macropores. Macropores in the surface soil, formed by soil fauna and the decay of plant roots, are a common feature of grasslands. Water can enter macropores when the surface soil layer is saturated or partially saturated (Weiler and Naef, 2003); consequently, the infiltration rate will increase. The increased infiltration rates in the latter half of the experiment may have reflected a change in water flow paths under such conditions.

Since these phenomena appeared to occur due to the high rainfall intensity of the simulated rain, the 3-min average of the minimum infiltration rate during a simulated rainfall experiment was used as the final infiltration rate for these sites. The resulting final infiltration rates were 34.5 mm h^{-1} for SB3, 47.1 mm h^{-1} for SK3, and 51.7 mm h^{-1} for SK4. Similarly, for the desert grassland and shrubland plots, the final infiltration rates were 34.1 mm h^{-1} for DM2, 84.3 mm h^{-1} for DM3, and 10.0 mm h^{-1} for SH1.

5.2. The role of surface vegetation cover in the infiltration rate

Fig. 8a and b shows the final infiltration rates plotted against the surface vegetation cover. On the steppe grassland, a higher infiltration rate (>80 mm h^{-1}) was observed on the ungrazed plots (SB1, SK1) with dense vegetation cover (>40%). For plots with lower vegetation cover, however, the infiltration rate was less than 40 mm h^{-1} at the BGN site and 50 mm h^{-1} or less at the KBU site. These results suggest that dense surface vegetation cover increases the infiltration rate significantly on steppe grassland; however, the relationship between surface vegetation cover and final infiltration rate was not statistically significant ($p=0.21$).

On the desert grassland, the infiltration rate varied considerably regardless of surface vegetation cover. For the ungrazed locations, the infiltration rate was relatively high (88.0 mm h^{-1}) for the DM1 plot, where sandy micromounds were formed on the soil surface; however, at the DM2 plot without micromounds, the infiltration rate was low (34.1 mm h^{-1}). In contrast, for the grazed locations, the surface cover conditions were similar but the infiltration rates differed considerably. Abrahams et al. (1988) reported that surface vegetation cover had a

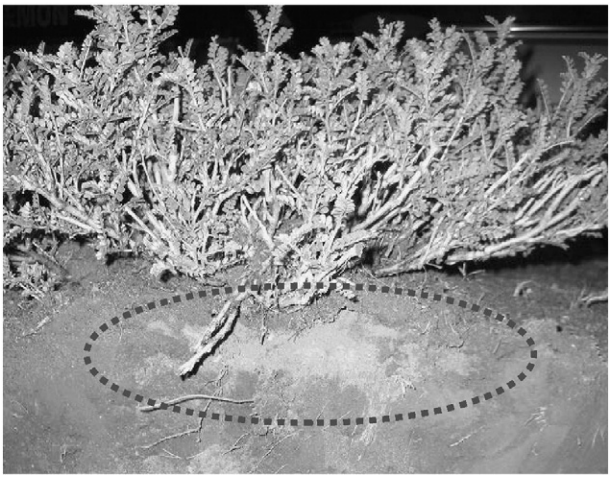

Fig. 7. Dry soil in sandy microdunes beneath the shrub canopy after the rainfall simulation experiment.

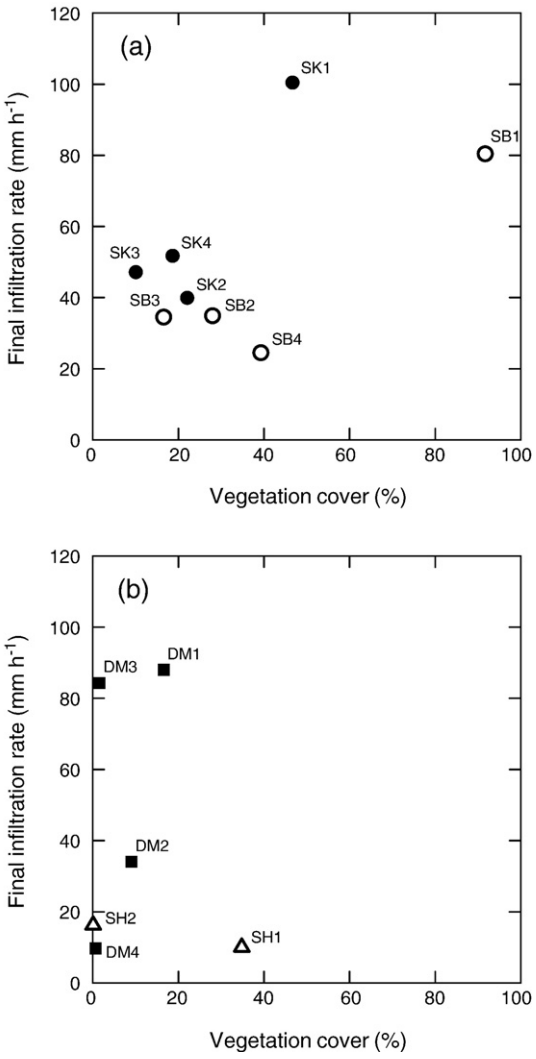

Fig. 8. Relationships between the surface vegetation cover and final infiltration rate at the (a) steppe grassland site and the (b) desert grassland and shrubland sites. Open and solid circles denote the BGN site and the KBU site, respectively. The solid square and open triangle indicate the desert grassland site and shrubland site, respectively. Steppe grassland ($y=0.58x+31.9$, $r^2=0.34$, $p=0.21$).

rather weak influence on the infiltration rate if the vegetation cover was sparse (<10%). Our results also suggest that surface vegetation cover has negligible influence on the infiltration rate in the desert grasslands of Mongolia, where the surface vegetation cover is very sparse.

For shrubland, infiltration rates were similarly low at both the shrub and intershrub plots. Previous studies have observed infiltration rates greater than 30 mm h^{-1} under shrub canopies (Parsons et al., 1996; Cerdà et al., 1998; Wainwright et al., 2000); however, we observed a low infiltration rate (10.0 mm h^{-1}) for the shrub plot as well as for the intershrub plot (16.2 mm h^{-1}). Water infiltration under a shrub canopy will differ depending on the size of the shrub canopy and the root distribution, which affect the throughfall distributions and the depth to which stemflow infiltrates via root channels (Martinez-Meza and Whitford, 1996). However, we found dry soils within the sandy microdunes beneath the shrub canopy after the rainfall simulation experiment (Fig. 7). Cerdà et al. (1998) reported that the heterogeneous wetting front beneath the shrub canopy was maintained by hydrophobicity of the surface soil. For the shrub plot in this study, hydrophobicity of the sandy dune soil was considered to be the cause of the limited water infiltration.

5.3. Relationships between total surface cover and the infiltration rate

The surface vegetation cover and final infiltration rate on the steppe grassland did not show a statistically significant relationship. Comparison of the infiltration rates between the KBU and BGN sites indicated that the infiltration rate at KBU was likely slightly higher than that at BGN at the same level of surface vegetation cover. Previous studies have reported that the infiltration rate of a stony surface depends on the cover percentage, size, and geometry of the stone covering the soil surface (Poesen, 1986; Valentin and Casenave, 1992). The soil surface at KBU was characterized by stone cover, namely gravel lags that were mostly on top of the surface but not buried in the soil. In such a case, the surface stone cover would have increased the infiltration rate to some extent by protecting the bare soil surface from raindrop impact and by damming surface flow (Poesen, 1986). Thus, not only the vegetation cover but also the stone cover should be considered when investigating the infiltration rate at sites covered with free gravel lags.

Fig. 9a and b shows infiltration rates plotted against the total surface cover, given as the total percentage of cover by vegetation and rock fragments on the soil surface. For the steppe grassland, the infiltration

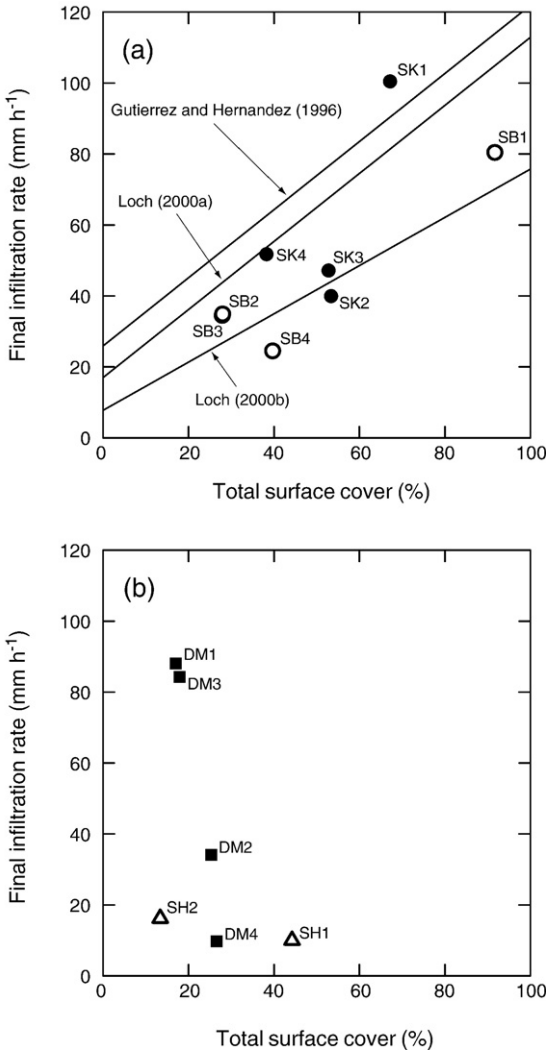

Fig. 9. Relationships between the total surface cover and the infiltration rate at the (a) steppe grassland site and the (b) desert grassland and shrubland sites. The open and solid circles denote the BGN site and KBU site, respectively. The solid square and open triangle indicate the desert grassland site and shrubland site, respectively. Steppe grassland ($y=0.92x+5.74$, $r^2=0.59$, $p=0.029$) and desert grassland ($y=-7.67x+220.4$, $r^2=0.98$, $p=0.042$) in Mongolia, and results by Gutierrez and Hernandez (1996) ($y=0.96x+25.9$), Loch (2000a) ($y=0.96x+17.0$), and Loch (2000b) ($y=0.68x+7.74$).

rate increased with the total surface cover at both sites (Fig. 9a). The statistically significant correlation between the total surface cover and the infiltration rate ($p=0.029$) suggested that the effect of total surface cover on the infiltration rate was fairly similar at both the BGN and KBU sites.

Cover by rock fragments clearly increased the infiltration rate on the steppe grassland; however, rock fragment cover may promote overland flow generation when free gravel is embedded in the soil (Valentin and Casenave, 1992). Thus, while rock fragment cover temporally increased the infiltration rate for our steppe grassland sites, the infiltration rates might decrease if changes were to occur in the position of rock fragments and the condition of the surrounding soil. Therefore, higher surface vegetation cover is desirable for maintaining the higher infiltration rate of the grassland.

Fig. 9b presents the relationships between the total surface cover and the final infiltration rate for desert grassland and shrubland. On the desert grassland, the infiltration rate tended to decrease as the total surface cover increased ($p=0.042$). The lower stone cover indicates the accumulation of sandy aeolian deposits, suggesting that high permeability of the sandy soil led to the higher infiltration rate. In contrast, for the shrubland, the infiltration rate was not markedly influenced by the surface cover conditions. Thus, it is likely that not the surface cover condition, but rather the soil properties such as microrelief at the soil surface, soil texture, and hydrophobicity of the soil surface, predominantly affect the infiltration rates of desert grassland and shrubland in Mongolia.

5.4. The role of surface cover in the infiltration rates of semiarid environments

Loch (2000a) measured infiltration rates using an oscillating nozzle rainfall simulator (raindrop kinetic energy was 29.5 J mm^{-1}) and a large runoff plot (1.5 m wide and 12 m long) on bund slopes in the Northparkes Mines of New South Wales, Australia. The bund slopes were revegetated by ryegrass, and the topsoil was sandy clay soil. Loch (2000b) also investigated the effect of surface vegetation cover on the infiltration rate on a hillslope, using the same method described above, in the subtropical environment of Tarong, southern Queensland, Australia. In contrast, Gutierrez and Hernandez (1996) investigated the role of surface vegetation cover on runoff generation from a grassy hillslope in the semiarid rangeland of northern Mexico. Simulated rainfall with raindrop kinetic energy of 11.3 J mm^{-1} was applied on a 1-m^2 plot with silty–clay loam topsoil using a drip-type rainfall simulator.

The relationships between the surface vegetation cover and final infiltration rate observed in those studies are shown in Fig. 9a, drawn as linear regression lines. The relationships between the surface vegetation cover (total surface cover for this study) and the infiltration rate showed approximate correspondence to the different grassy hillslopes. The experiment by Gutierrez and Hernandez (1996) tended to have slightly higher infiltration rates; this was possibly due to the lower raindrop kinetic energy of simulated rainfall, as laboratory experiments have demonstrated that the final infiltration rate decreases as the intensity of simulated rainfall increases (Agassi et al., 1994). Nevertheless, the high consistency in these relationships suggest rather common effects of surface cover on the infiltration rate throughout grass-covered hillslopes in semiarid environments.

5.5. Mechanism of infiltration-rate recovery after short-term livestock exclusion

At both the BGN and KBU sites, the infiltration rates were higher on the ungrazed plots, where grazing had been prohibited for 4 years. The difference between the ungrazed and grazed plots was 55.4 mm h^{-1} for the BGN site and 60.4 mm h^{-1} for the KBU site. The differences in the surface vegetation cover between the ungrazed and grazed plots at BGN and KBU were 64.7 and 24.6%, respectively. The plots, however, had substantially the same topsoil penetration resistance (Fig. 10).

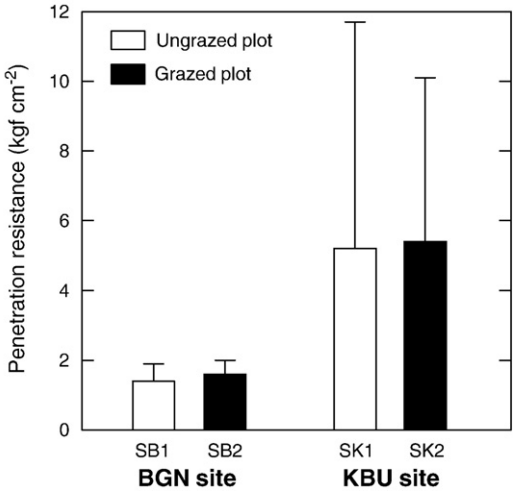

Fig. 10. Penetration resistance of the topsoil for the ungrazed and grazed plots. Error bars represent the standard deviations of the measured values.

Rietkerk et al. (1997) suggested that the recovery of the infiltration rate on degraded grassland occurred with the recovery of surface vegetation cover. Meanwhile, Castellano and Valone (2007) examined the recovery of livestock-compacted, degraded grassland based on infiltration-rate measurements using a double-ring infiltrometer; they reported that the infiltration rate increased with recovery following long-term removal of the livestock. However, the infiltration rate in their study might not have changed under the raindrop impact of natural rainfall because surface vegetation had not recovered at their study sites.

In this study, the penetration resistance of topsoil indicated that the soil structure had not yet been changed by the short-term livestock removal; nevertheless, the ungrazed site had a higher infiltration rate than the grazed site. We observed the development of cracks on the residual crust surface under the canopy, which could have increased water infiltration into the crusted soil (Stolte et al., 1997; Wells et al., 2003). Canopy cover by surface vegetation generally reduces direct raindrop impacts onto a bare soil surface and hence prevents surface sealing and crusting; therefore, although soil hardness had not changed following short-term livestock removal, the microscopic structure of the soil surface may have had recovered to some extent. That is, the high infiltration rates for the ungrazed plots seemed to be maintained by the recovery of surface vegetation cover.

The infiltration rates of the ungrazed sites showed a relationship between the total surface cover and the infiltration rate, which appears to be common throughout grassy hillslopes (Fig. 9a). This implies that infiltration rates in the study area can recover via short-term exclusion of livestock. For steppe grassland in Mongolia, to understand the mechanisms of recovery from desertification processes, assessing the infiltration-rate recovery in response to livestock removal is necessary. Rainfall experiments that simulate natural rainfall and its raindrop impacts can help clarify these mechanisms.

6. Conclusions

A series of field infiltration tests was conducted using a modified oscillating nozzle rainfall simulator and small plots on steppe grassland, desert grassland, and shrubland in semiarid areas of Mongolia. The final infiltration rates ranged from 24.5 to 100.4 mm h^{-1} for the steppe grassland, 9.7 to 88.0 mm h^{-1} for the desert grassland, and 10.0 to 14.3 mm h^{-1} for the shrubland. The steppe grassland with relatively dense vegetation cover had significantly higher final infiltration rates. However, the effect of surface vegetation cover was rather small on the desert grassland and shrubland. On the steppe grassland, a statistically significant correlation was observed between the total surface cover

and the final infiltration rate, suggesting that the rock fragment cover on the soil surface increased the infiltration rate to some extent. The relationship between the total surface cover and the final infiltration rate obtained for the steppe grassland was fairly similar to the relationship between the surface vegetation cover and final infiltration rates reported for grassy hillslopes in various other regions; this implies that the effect of surface cover on the final infiltration rate is rather common for grassy hillslopes. Short-term livestock removal on the Mongolian steppe grassland resulted in the recovery of the surface vegetation cover and hence increased the final infiltration rate significantly. The infiltration rates of the ungrazed plots likely recovered to the initial condition; this result implies that currently, the steppe grassland of Mongolia can recover from the desertification process. To understand the potential recovery mechanisms of degraded grassland from desertification, we must investigate the response of the infiltration rate to livestock removal through series of field infiltration tests that simulate raindrop impacts.

References

Abrahams, A.D., Parsons, A.J., Luk, S., 1988. Hydrological and sediment responses to simulated rainfall on desert hillslopes in southern Arizona. Catena 15, 103–117.

Abu-Awwad, A.M., Shatanawi, M.R., 1997. Water harvesting and infiltration in arid areas affected by surface crust: examples from Jordan. Journal of Arid Environment 37, 443–452.

Agassi, M., Bloem, D., BenHur, M., 1994. Effect of drop energy and soil and water chemistry on infiltration and erosion. Water Resources Research 30 (4), 1187–1193.

Asano, M., Tamura, K., Kawada, K., Higashi, T., 2007. Morphological and physico-chemical characteristics of soils in a steppe region of the Kherlen River basin, Mongolia. Journal of Hydrology 333, 100–108.

Bayasgolan, M., Dagvadorj, D., 2005. Desertification monitoring using remote sensing data. Proceedings of the First International Symposium on Terrestrial and Climate Change in Mongolia. Ulaanbaatar, Mongolia, pp. 176–178.

Begzsuren, S., Ellis, J.E., Ojima, D.S., Coughenour, M.B., Chuluun, T., 2004. Livestock responses to droughts and severe winter weather in the Gobi Three Beauty National Park, Mongolia. Journal of Arid Environments 59, 785–796.

Blackburn, W.H., 1975. Factors influencing infiltration and sediment production of semiarid rangelands in Nevada. Water Resources Research 11 (6), 929–937.

Brazier, R.E., Parsons, A.J., Wainwright, J., Powell, D.M., Schlesinger, W.H., 2007. Upscaling understanding of nitrogen dynamics associated with overland flow in a semi-arid environment. Biogeochemistry 82, 265–278.

Castellano, M.J., Valone, T.J., 2007. Livestock, soil compaction and water infiltration rate: evaluating a potential desertification recovery mechanism. Journal of Arid Environments 71, 97–108.

Cerdà, A., Schnabel, S., Ceballos, A., Gomez-Amelia, D., 1998. Soil hydrological response under simulated rainfall in the Dehesa land system (Extremadura, SW Spain) under drought conditions. Earth Surface Processes and Landforms 23, 195–209.

Chen, Y., Lee, G., Lee, P., Oikawa, T., 2006. Model analysis of grazing effect on above-ground biomass and above-ground net primary production of a Mongolian grassland ecosystem. Journal of Hydrology 333, 155–164.

Chuluun, T., Ojima, D., 2001. Sustainability of pastoral systems in Mongolia. Proceedings of the Open Symposium on Change and Sustainability of Pastoral Land Use Systems in Temperate and Central Asia. Ulaanbaatar, Mongolia, pp. 52–57.

Dadkhah, M., Gifford, G.F., 1980. Influence of vegetation, rock cover, and trampling on infiltration rates and sediment production. Water Resources Bulletin 16 (6), 979–986.

Dunne, T., Zhang, W., Aubry, B.F., 1991. Effects of rainfall, vegetation, and microtopography on infiltration and runoff. Water Resources Research 27 (9), 2271–2285.

Evans, R., 1980. Mechanics of water erosion and their spatial and temporal controls: an empirical viewpoint. In: Kirkby, M.J., Morgan, R.P.C. (Eds.), Soil Erosion. John Wiley and Sons Ltd., pp. 109–128.

Gibbens, R.P., Beck, R.F., Mcneely, R.P., Herbel, C.H., 1992. Recent rates of mesquite establishment in the northern Chihuahuan desert. Journal of Range Management 45 (6), 585–588.

Gutierrez, J., Hernandez, I.I., 1996. Runoff and interrill erosion as affected by grass cover in a semi-arid rangeland of northern Mexico. Journal of Arid Environments 34, 287–295.

Hennessy, J.T., Gibbens, R.P., Tromble, J.M., Cardenas, M., 1983. Vegetation changes from 1935 to 1980 in mesquite dunelands and former grassland of southern New Mexico. Journal of Range Management 36 (3), 370–374.

Kato, H., Onda, Y., Ito, S., Nanko, k., 2008. Field measurement of infiltration rate using an oscillating nozzle rainfall simulator in devastated Hinoki plantation. Journal of Japan Society of Hydrology and Water Resources 21 (6), 439–448 (in Japanese with English Abstr.).

Loch, R.J., 2000a. Using rainfall simulation to guide planning and management of rehabilitated areas: part I. Experimental methods and results from a study at the Northparkes Mine, Australia. Land Degradation & Development 11, 221–240.

Loch, R.J., 2000b. Effects of vegetation cover on runoff and erosion under simulated rain and overland flow on a rehabilitated site on the Meandu Mine, Tarong, Queensland. Australian Journal of Soil Research 38, 299–312.

Martinez-Meza, E., Whitford, W.G., 1996. Stemflow, throughfall and channelization of stemflow by roots in three Chihuahuan desert shrubs. Journal of Arid Environments 32, 271–287.

Meyer, L.D., Harmon, W.C., 1979. Multiple-intensity rainfall simulator for erosion research on row sideslopes. Transactions of the ASAE 22, 100–103.

Mills, A.J., Fey, M.V., 2004. Effects of vegetation cover on the tendency of soil to crust in South Africa. Soil Use and Management 20, 308–317.

Munkhtsetseg, E., Kimura, R., Wang, J., Shinoda, M., 2007. Pasture yield response to precipitation and high temperature in Mongolia. Journal of Arid Environments 70 (1), 94–110.

Murai, H., Iwasaki, Y., 1975. Studies on function of water and soil conservation based on forest land (I) – Influence of difference in forest condition upon water run-off, infiltration and soil erosion. Bulletin of the Government Forest Experiment Station 274, 23–84 (in Japanese with English Abstr.).

Nanko, K., Hotta, N., Suzuki, M., 2004. Assessing raindrop impact energy at the forest floor in a mature Japanese cypress plantation using continuous raindrop-sizing instruments. Journal of Forest Research 9, 157–164.

Neave, M., Abrahams, A.D., 2002. Vegetation influences on water yields from grassland and shrubland ecosystems in the Chihuahuan desert. Earth Surface Processes and Landforms 27, 1011–1020.

Nishikawa, T., Onda, Y., Tanaka, Y., Kato, H., Tsujimura, M., Seki, R., Asano, M., Davaa, G., Oyunbaatar, D., 2005. Estimating soil erosion rates using Cs-137 in Eastern Mongolia. Journal of the Japanese Society of Erosion Control Engineering 58 (3), 4–14 (in Japanese with English Abstr.).

Onda, Y., Kato, H., Tanaka, Y., Tsujimura, M., Davaa, G., Oyunbaatar, D., 2007. Analysis of runoff generation and soil erosion processes by using environmental radionuclides in semiarid areas of Mongolia. Journal of Hydrology 333, 124–132.

Parsons, A.J., Abrahams, A.D., Wainwright, J., 1996. Response of interrill runoff and erosion rates to vegetation change in southern Arizona. Geomorphology 14, 311–317.

Poesen, J., 1986. Surface sealing as influenced by slope angle and position of simulated stones in the top layer of loose sediments. Earth Surface Processes Landforms 11, 1–10.

Rietkerk, M., van den Bosch, F., van de Koppel, J., 1997. Site-specific properties and irreversible vegetation changes in semi-arid grazing systems. Oikos 80, 241–252.

Rietkerk, M., Ketner, P., Burger, J., Hoorens, B., Olff, H., 2000. Multiscale soil and vegetation patchiness along a gradient of herbivore impact in a semi-arid grazing system in West Africa. Plant Ecology 148, 207–224.

Ritchie, J.C., Herrick, J.E., Ritchie, C.A., 2003. Variability in soil redistribution in the northern Chihuahuan Desert based on ^{137}Cesium measurements. Journal of Arid Environments 55, 737–746.

Saandar, M., Sugita, M., 2004. Digital atlas of Mongolian natural environments (1) vegetation, soil, exosystem and water. CD-ROM, Monmap Engineering Service Co., Ltd, Ulaanbaatar 210646, Mongolia.

Schlesinger, W.H., Abrahams, A.D., Parsons, A.J., Wainwright, J., 1999. Nutrient losses in runoff from grassland and shrubland habitats in Southern New Mexico: I. rainfall simulation experiments. Biogeochemistry 45, 21–34.

Seeger, M., 2007. Uncertainty of factors determining runoff and erosion processes as quantified by rainfall simulations. Catena 71, 56–67.

Stolte, J., Ritsema, C.J., de Roo, A.P.J., 1997. Effects of crust and cracks on simulated catchment discharge and soil loss. Journal of Hydrology 195, 279–290.

Sugita, M., Asanuma, J., Tsujimura, M., Mariko, S., Lu, M., Kimura, F., Azzaya, D., Adyasuren, T., 2007. An overview of the rangelands atmosphere–hydrosphere–bioshere interaction study experiment in northeastern Asia (RAISE). Journal of Hydrology 333, 3–20.

Thurow, T.L., Blackburn, W.H., Taylor Jr., C.H., 1986. Hydrological characteristics of vegetation types as affected by livestock grazing systems, Edwards Plateau Texas. Journal of Range Management 39, 505–509.

Valentin, C., Casenave, A., 1992. Infiltration into sealed soils as influenced by gravel cover. Soil Science Society of America Journal 56, 1667–1673.

Wainwright, J., Parsons, A.J., Abrahams, A.D., 2000. Plot-scale studies of vegetation, overland flow and erosion interactions: case studies from Arizona and New Mexico. Hydrological Processes 14, 2921–2943.

Weiler, M., Naef, F., 2003. Simulating surface and subsurface initiation of macropore flow. Journal of Hydrology 273, 139–154.

Wells, R.P., DiCarlo, D.A., Steenhuis, T.S., Parlange, J.Y., Romkens, M.J.M., Prasad, S.N., 2003. Infiltration and surface geometry features of a swelling soil following successive simulated rainstorms. Soil Science Society of America Journal 67, 1344–1351.